

The Cosmic Star Formation History: Insights from Kilonova-Associated Gamma-Ray Bursts

QIN-MEI LI,¹ QI-BIN SUN,¹ SHENG-BANG QIAN,¹ SI-YUAN ZHU,² AND FU-XING LI¹

¹*Department of Astronomy, School of Physics and Astronomy, Yunnan University, Kunming 650091, China*

²*School of Physics and Astronomy, Sun Yat-Sen University, Zhuhai, 519082, China*

ABSTRACT

The origin of the Universe and its material content remains one of the most fundamental questions in science. Gamma-ray bursts (GRBs), with their extreme luminosities and high-redshift detectability, provide a unique window into the history of cosmic formation and chemical evolution. Consequently, the GRB formation rate (FR) has been employed to trace the star formation rate (SFR) across cosmic time. GRBs are conventionally classified into long and short categories (lGRBs and sGRBs) based on their T_{90} duration. sGRBs are widely employed as tracers of the delayed SFR, owing to their origin linked to the inspiral timescales of compact binary systems. However, some studies suggest that the detection of supernova-associated sGRBs may indicate potential contamination by core-collapse events. In this work, we move beyond the T_{90} classification and focus exclusively on GRBs with confirmed kilonova signatures, which provide unambiguous evidence of binary compact star mergers, to reassess their connection with the delayed SFR. Through analysis of a kilonova-associated GRB (KN/GRBs) sample, we find that even within this robust subset, the KN/GRB FR displays a trend contrary to that of the delayed SFR at low redshifts ($z < 1$). This result challenges the conventional theory by indicating that low-redshift KN/GRBs may not accurately trace the delayed SFR, independent of core-collapse contamination, while further validation with larger KN/GRB samples is essential to determine the reliability of compact binary mergers as probes of delayed SFR.

Keywords: Gamma-ray bursts(629); Star formation(1569); Luminosity function(942);

1. INTRODUCTION

Gamma-ray bursts (GRBs) are among the most energetic astrophysical events in the universe, characterized by intense bursts of high-energy photons. Based on the bimodal distribution of GRBs in the duration–spectral hardness diagram (Kouveliotou et al. 1993), GRBs are generally classified into two categories: long-duration, soft-spectrum GRBs (lGRBs) and short-duration, hard-spectrum GRBs (sGRBs). These two populations are widely believed to originate from distinct progenitor systems. lGRBs are commonly associated with the core collapse of Wolf–Rayet stars (Woosley 1993; Paczyński 1998; MacFadyen & Woosley 1999), supported by direct observational evidence linking lGRBs to supernovae (SN; Stanek et al. 2003; Zeh et al. 2004; Kann et al. 2024). sGRBs are predominantly associated with the mergers of compact binary systems, such as binary neutron stars (BNS) or neutron star–black hole (NS–BH) binaries (Paczynski 1986; Eichler et al. 1989; Narayan et al. 1992). The detection of GW170817 and its electromagnetic counterparts—GRB 170817A and the optical transient AT 2017gfo—provided compelling observational evidence that BNS mergers can give rise to sGRBs (Abbott et al. 2017a). Subsequently, continued observations of AT 2017gfo led to its identification as a kilonova (KN) (Arcavi et al. 2017; Abbott et al. 2017b; Kasen et al. 2017). KN are transient astronomical events powered by the radioactive decay of heavy r-process elements synthesized in the predominantly isotropic ejecta produced during the merger of BNS or NS–BH systems. The high-energy decay photons are trapped within the expanding ejecta, leading to thermalization and the production of broadband optical–infrared radiation similar to that of a supernova (SN), but with peak luminosities intermediate between those of classical novae and core-collapse SN(Li & Paczyński 1998; Rosswog 2005; Metzger 2017).

GRBs are often considered tracers of the cosmic star formation rate (SFR), as they originate from the remnants of massive stars. These compact remnants form shortly after the birth of the most massive stars, during their final evolutionary stages, linking GRBs to episodes of active star formation (Wijers et al. 1998; Totani 1997; Blain & Natarajan 2000; Elliott et al. 2012). However, in the case of compact binary mergers, a time delay between the SFR and the merger rate is expected due to the orbital inspiral timescale (Ando 2004; Piran & Guetta 2006; Wanderman & Piran 2015). As a result, sGRBs are increasingly viewed as potential tracers of delayed SFR.

The intrinsic durations ($T_{90}/(1+z)$) of GRB 080913 (Greiner et al. 2009) and GRB 090423 (Tanvir et al. 2009; Salvaterra et al. 2009) are less than 2 s, yet evidence suggests their origins are consistent with massive stars (Zhang et al. 2009). Bromberg et al. (2013) suggested that a substantial fraction, up to approximately 40%, of sGRBs detected by *Swift* may originate from collapsars rather than compact binary mergers, indicating contamination of the canonical short GRB population. Petrosian & Dainotti (2024) found that a subset of lGRBs with higher event rates exhibit a tendency to align with a delayed SFR model. This correlation leads them to propose that low-redshift lGRBs may, in part, originate from the mergers of compact binary systems. Du et al. (2025) proposed event rates of sGRBs can be described by both the delay and undelayed SFR model, suggesting that a subset of sGRBs may originate from the core collapse of massive stars rather than from compact binary mergers.

Although the correlations between lGRBs - SN and sGRBs - KN provide strong support for the collapsar and compact binary merger models, respectively, a number of exceptions have emerged that complicate this simple classification. Notably, the lGRBs 060614 (Gehrels et al. 2006) and 060505 (Fynbo et al. 2006) lack detectable SN signatures but instead show features consistent with KN emission. Likewise, sGRB 200826A ($T_{90} = 1.16$ s) was found to be accompanied by a SN (Ahumada et al. 2021; Zhang et al. 2021), challenging the canonical expectation for sGRB. Moreover, recent studies have confirmed KN associations with several lGRBs—GRB 060505 (Jin et al. 2021), GRB 080503A (Zhou et al. 2023), GRB 211211A (Yang et al. 2022), and GRB 230307A (Wang et al. 2023)—which are now believed to originate from mergers of compact binary systems.

These findings collectively suggest that a fraction of sGRBs may originate from core-collapse events. Moreover, evidence is emerging that compact binary mergers, traditionally associated with sGRBs, may also contribute to a subset of lGRBs. This indicates that the progenitor channels of both sGRBs and lGRBs are more interconnected and complex than previously thought. As a result, the traditional classical method is no longer universally valid. The link between sGRBs and compact binary mergers should be reconsidered. This undermines the reliability of using T_{90} -based sGRBs as tracers of the delay SFR. To address this issue, this paper proposes that GRBs directly associated with kilonovae (KN/GRBs) should be used as more reliable tracers of the cosmic delay SFR. By focusing on this subset of GRBs, we can obtain a cleaner progenitor population, minimizing contamination from core-collapse events. This approach offers a more robust foundation for utilizing GRBs in cosmological studies.

This paper is organized as follow. In Section 2, we introduce sample selection and data analysis method. In Section 3, we show the result of luminosity function (LF) and FR for 19 KN/GRBs. The conclusion and discussion are displayed in Section 4. Throughout the paper, we assume a flat Λ universe with $\Omega_m = 0.3$ and $H_0 = 70 \text{ km s}^{-1} \text{Mpc}^{-1}$.

2. SAMPLE SELECTION AND DATA ANALYSIS METHOD

2.1. Sample Selection

We collected a sample that have been confirmed to be associated with KN from the literature, of which 15 were drawn from Li et al. (2023), while the remaining sources were selected from various previously published studies. This sample includes multi-band observational data, light curve characteristics, and redshift measurements, providing a valuable statistical basis for investigating the properties of KN and their connection to host galaxies. Jin et al. (2021) reported a thermal-like optical radiation component in GRB 060505, which can be interpret as a blue KN. GRB 211211A was discovered in likely association with a galaxy at $z=0.076$ (Rastinejad et al. 2022). Zhu et al. (2023) found the light-curve behaviour of GRB 070707 can be explained as an external forward shock afterglow component plus a KN, Yang et al. (2024) reported a lanthanide-rich KN in the aftermath of GRB 230307A. Stratta et al. (2025) provided evidence for KN Light for GRB 191019A by joint of an afterglow plus a KN model revealed a better match than an afterglow-only scenario, the resulting KN properties resemble those of AT2017gfo associated with the binary neutron star merger GW170817. Our sample is enlarge to 20 KN/GRBs used to determine the LF and FR. Combining main spectral data from literature and the Gamma-ray Burst Coordinates Network¹.

¹ <https://www.mpe.mpg.de/~jcg/grbgen.html>

Table 1 provided the parameters information, including name, duration T_{90} , redshift, low-high energy power-law index α and β , peak energy E_p of the vfv spectrum in the observer's frame, peak flux F , energy band, bolometric luminosity, and references of KN/GRBs. Figure 1 (a) displays the T_{90} duration distribution for our KN/GRBs sample. Notably, 8 bursts exhibit durations longer than the conventional 2 s threshold. This observation, combined with the known population of long-duration ($T_{90} > 2$ s) events originating from compact binary mergers (as discussed in previous sections), further demonstrates the limitations of using T_{90} as a definitive progenitor classification criterion.

2.2. Luminosity calculate

The bolometric peak luminosity L of a GRB are calculate by using:

$$L = 4\pi d_L^2(z)FK, \quad (3)$$

where $d_L(z)$ is the luminosity distance at redshift z , defined as:

$$d_L(z) = \frac{c}{H_0} (1+z) \int_0^z \frac{dz'}{\sqrt{1-\Omega_m + \Omega_m(1+z')^3}}, \quad (4)$$

F is the peak flux observed between energy ranges (E_{\min} , E_{\max}), and K is the K-correction factor, since the peak fluxes of GRBs are observed over a wide range of redshifts, corresponding to different rest-frame energy bands, we need to make K-correction transform the observed band of telescope in to 1-10⁴ keV band to obtain the bolometric luminosity of GRBs (Bloom et al. 2001). If the F is in units of erg cm⁻² s⁻¹, then the parameter K is defined as:

$$K = \frac{\int_{1 \text{ keV}/(1+z)}^{10^4 \text{ keV}/(1+z)} Ef(E) dE}{\int_{E_{\min}}^{E_{\max}} Ef(E) dE}. \quad (5)$$

If the flux F is in units of photons cm⁻² s⁻¹, then the parameter K is defined as:

$$K = \frac{\int_{1 \text{ keV}/(1+z)}^{10^4 \text{ keV}/(1+z)} Ef(E) dE}{\int_{E_{\min}}^{E_{\max}} f(E) dE}. \quad (6)$$

$f(E)$ denotes the spectral model of GRBs. there are two spectral models are employed to fit the spectra of GRBs: a power law with an cutoff exponential model (CPL; Sakamoto et al. 2008) and the Band model (Band et al. 1993). The functional forms of these models are as follows: The CPL model can be expressed as

$$f(E) = A \left(\frac{E}{100 \text{ keV}} \right)^\alpha \exp \left(-\frac{(2+\alpha)E}{E_p} \right), \quad (1)$$

where A is the normalization factor, α is the power-law index, and E_p is the peak energy in observer frame. The GRBs are best fitted with Band model can be written as:

$$f(E) = \begin{cases} A \left(\frac{E}{100 \text{ keV}} \right)^\alpha \exp \left(-\frac{(2+\alpha)E}{E_p} \right), & E < \frac{(\alpha-\beta)E_p}{2+\alpha}, \\ A \left(\frac{E}{100 \text{ keV}} \right)^\beta \exp \left[(\beta-\alpha) \left(\frac{(\alpha-\beta)E_p}{(2+\alpha)100 \text{ keV}} \right)^{\alpha-\beta} \right], & E \geq \frac{(\alpha-\beta)E_p}{2+\alpha}, \end{cases} \quad (2)$$

where A is the normalization factor, α and β are the low- and high-energy photon indices, respectively. It should be noted that the bursts in our sample were detected by instruments aboard different satellites. To ensure that all bursts in the sample are above the flux limit, we adopt the best sensitivity of $F_{\text{limit}} = 1 \times 10^{-8}$ erg cm⁻²s⁻¹ for KN/GRBs as the flux threshold for the entire sample (Wu et al. 2012; Li et al. 2025). Hence, the corresponding luminosity limit at redshift z can be calculated using $L_{\text{limit}} = 4\pi d_L^2(z)F_{\text{limit}}$.

2.3. Delay time model

With the binary merger scenario as a guiding framework, a rate function that accounts for a time delay relative to the SFR was constructed (Totani 1999; Ando 2004; Piran & Guetta 2006; Wanderman & Piran 2015). This delayed rate is formulated as the convolution between a given SFR model and a delay-time distribution, $f(\Delta t)$, which represents the

probability distribution of time delays relative to the SFR. The intrinsic KN/GRBs rate is expressed as the convolution of the SFR with the delay-time distribution $f(\Delta t)$.

$$R_{\text{sGRB}}(z) \propto \int_{z_{\min}}^{\infty} \text{SFR}(z') \left(f(t(z) - t(z')) \frac{d\tau}{dz'} \right) dz'. \quad (1)$$

where $z_{\min}(z)$ is obtained on solving $t_z - t_{z_{\min}} = \tau_{\min} = 10$ Myr (Paul 2018).

Here, we use the SFR model of Madau & Dickinson (2014), which can be expressed as

$$\text{SFR}(z) = \frac{(1+z)^{2.7}}{1 + \left(\frac{1+z}{2.9}\right)^{5.6}}, \quad (2)$$

We consider three models for the time delay (Sun et al. 2015):

(1) Gaussian merger delay time-scale model. The probability intensity distribution as

$$f(\tau) = \frac{1}{\sigma\sqrt{2\pi}} \exp\left(-\frac{(\tau - \tau_0)^2}{2\sigma^2}\right), \quad (3)$$

where $\tau_0 = 2$ Gyr, and $\sigma = 0.3$ Gyr.

(2) Log-normal merger delay time-scale model

$$f(\tau) d\ln \tau = \frac{1}{\sigma\sqrt{2\pi}} \exp\left(-\frac{(\ln \tau - \ln \tau_0)^2}{2\sigma^2}\right) d\ln \tau, \quad (4)$$

where $\tau_0 = 2.9$ Gyr, and $\sigma = 0.2$ Gyr.

(3) Power-law merger delay time-scale model

$$f(\tau) = \tau^{-\alpha_\tau}, \quad (5)$$

where $\alpha_\tau = 0.81$. $\tau = t(z) - t(z')$ is the delay time between the formation and the merger of binary star systems. The $t(z)$ is age of the Universe calculated in a flat Λ universe (Lin et al. 2024), which is calculate as

$$t(z) = H_0^{-1} \int_z^{\infty} \left[(1+z') \sqrt{\Omega_m(1+z')^3 + \Omega_\Lambda} \right]^{-1} dz', \quad (6)$$

we plot the distribution of KN/GRBs rate based on the above three model in Figure 3.

2.4. Lynden-Bell's c^- method

Several selection effects influence the observed redshift distribution of GRBs (Coward 2007), and consequently their inferred event rate. The most significant of these arises from the observational limitations of satellite. These satellite has a flux limit, meaning that it is unable to detect GRBs fainter than a given threshold. As a result, the observed sample is truncated, and the intrinsic redshift distribution of GRBs cannot be reliably determined without first accounting for these observational biases.

Lynden-Bell (1971) (Lynden-Bell's c^-) putted forward a non-parametric methods that can be used to study the LF and density evolution for quasar sample. But Petrosian (1992) pointed that the drawback of non-parametric method is *ad hoc* assumption of *uncorrelated variables*. To overcoming this defects, Efron & Petrosian (1992) (EP) developed a new method (EP-L method) to test whether luminosity (L) and redshift (z) are correlated or not. This method is used on a variety of cosmological objects, such as quasar (Lynden-Bell 1971; Efron & Petrosian 1992), Active galactic nucleus (Maloney & Petrosian 1999; Singal et al. 2014; Zeng et al. 2021), GRBs (Yu et al. 2015; Petrosian et al. 2015; Li & Sun 2025), and FRB (Deng et al. 2019; Chen et al. 2024). In this paper, we also use this method to drive the cosmological evolution of LF and FR of our sample.

In Figure 1 (b), it is easy see that luminosity and redshift are dependent. Therefore, we need to eliminate this effect at first by using EP-L method (Efron & Petrosian 1992). Luminosity evolves with function $g_k(z) = (1+z)^k$, we can determine the value of k . As pointed as previous author (Efron & Petrosian 1992; Yu et al. 2015; Deng et al. 2019), we use the kendall τ statistical method to drive the k . Figure 1 (b) show the distribution of luminosity and redshift, for a random point i (z_i, L_i) in this plane, the J_i can be defined as

$$J_i = \{j | L_j \geq L_i, z_j \leq z_i^{\max}\} \quad (7)$$

where L_i is the luminosity of i th KN/GRB and z_i^{\max} is the maximum redshift at which the KN/GRBs with the luminosity limit. The range of J_i is shown as the black rectangle in Figure 1 (b). The number of KN/GRBs that contained in this region is defined as n_i . The number $N_i = n_i - 1$, which means takeing the i th point out. Similarly, the J'_i can be defined as

$$J'_i = \{j | L_j \geq L_i^{\lim}, z_j \leq z_i\} \quad (8)$$

where L_i^{\lim} is the limiting corrected gamma-ray luminosity at redshift z_i . In Figure 1 (b), the range of J'_i is shown as red rectangle. The number of KN/GRBs that contained in this range is defined as M_i .

Firstly, we consider to define the number of KN/GRBs that have redshift z less than or equal to z_i in black rectangle as R_i . The statistic τ is (Efron & Petrosian 1992)

$$\tau = \frac{\sum_i (R_i - E_i)}{\sqrt{\sum_i V_i}} \quad (9)$$

where $E_i = \frac{1+ni}{2}$ and $V_i = \frac{n_i^2-1}{12}$ are the expected mean and the variance for the hypothesis of independence, respectively. If R_i is exactly uniformly distributed between 1 and n_i , then the samples with $R_i \leq E_i$ and $R_i \geq E_i$ should be approximately equal in number, and the test statistic τ will be close to zero. If we choose a functional form of $g(z) = (1+z)^k$ that make the test statistic $\tau = 0$, then the effect of luminosity evolution can be removed by applying the transformation $L_0 = L/g(z)$. Figure 1 (d) show the distribution of non-evolving gamma-ray luminosity. The k value is 6.46 for 20 KN/GRBs, as shown in Figure 1 (c).

After eliminate the effect of the luminosity evolution, we can obtain the cumulative luminosity function with non-parametric method from following equation

$$\psi(L_{0i}) = \prod_{j < i} \left(1 + \frac{1}{N_j}\right) \quad (10)$$

and the cumulative number distribution can be derived from

$$\phi(z) = \prod_{j < i} \left(1 + \frac{1}{M_j}\right) \quad (11)$$

The differential form of $\phi(z)$ represents the formation rate of ρ , which can be expressed as

$$\rho(z) = \frac{d\phi(z)}{dz} (1+z) \left(\frac{dV(z)}{dz} \right)^{-1} \quad (12)$$

where $\frac{dV(z)}{dz}$ represents the differential comoving volume, which can be written as

$$\frac{dV(z)}{dz} = 4\pi \left(\frac{c}{H_0} \right) \frac{D_L^2}{(1+z)^2} \times \frac{1}{\sqrt{1 - \Omega_m + \Omega_m(1+z)^3}} \quad (13)$$

3. RESULT

In this section, we present the derived LF and FR for our KN/GRBs sample. Following the methodology described in previous sections, we quantify the luminosity evolution through a non-parametric approach using the Kendall τ correlation test. We use broken power law to fit the cumulative luminosity function in Figure 2 (a), and the following results were obtained:

$$\psi(L_0) \propto \begin{cases} L_0^{-0.15 \pm 0.04}, & L_0 < L_0^b \\ L_0^{-0.43 \pm 0.03}, & L_0 > L_0^b \end{cases} \quad (14)$$

where $L_0^b = (1.15 \pm 0.85) \times 10^{49} \text{ erg s}^{-1}$ is the break point. It is worth to point out that the $\psi(L/g(z))$ is local luminosity at $z = 0$ for the luminosity evolution is removed, and the luminosity function can be rewrite as $\psi(L_0) = \psi(L/(1+z)^{6.46})$. Therefore, the break luminosity at z can be deduced $L_z^b = L_0^b(1+z)^{6.46}$.

Figure 2 (b) displays the cumulative redshift distribution $\phi(z)$ for our sample. Prior to deriving the FR, we first obtain the differential form $d\phi(z)/dz$ through numerical differentiation. The error bar gives a 1σ poisson error (Gehrels 1986). As evident in Figure 3, the resulting FR $\rho(z)$ exhibits a pronounced decreasing trend with increasing redshift. When compared to the SFR and delay SFR, our results shows low redshifts excess ($z < 1$).

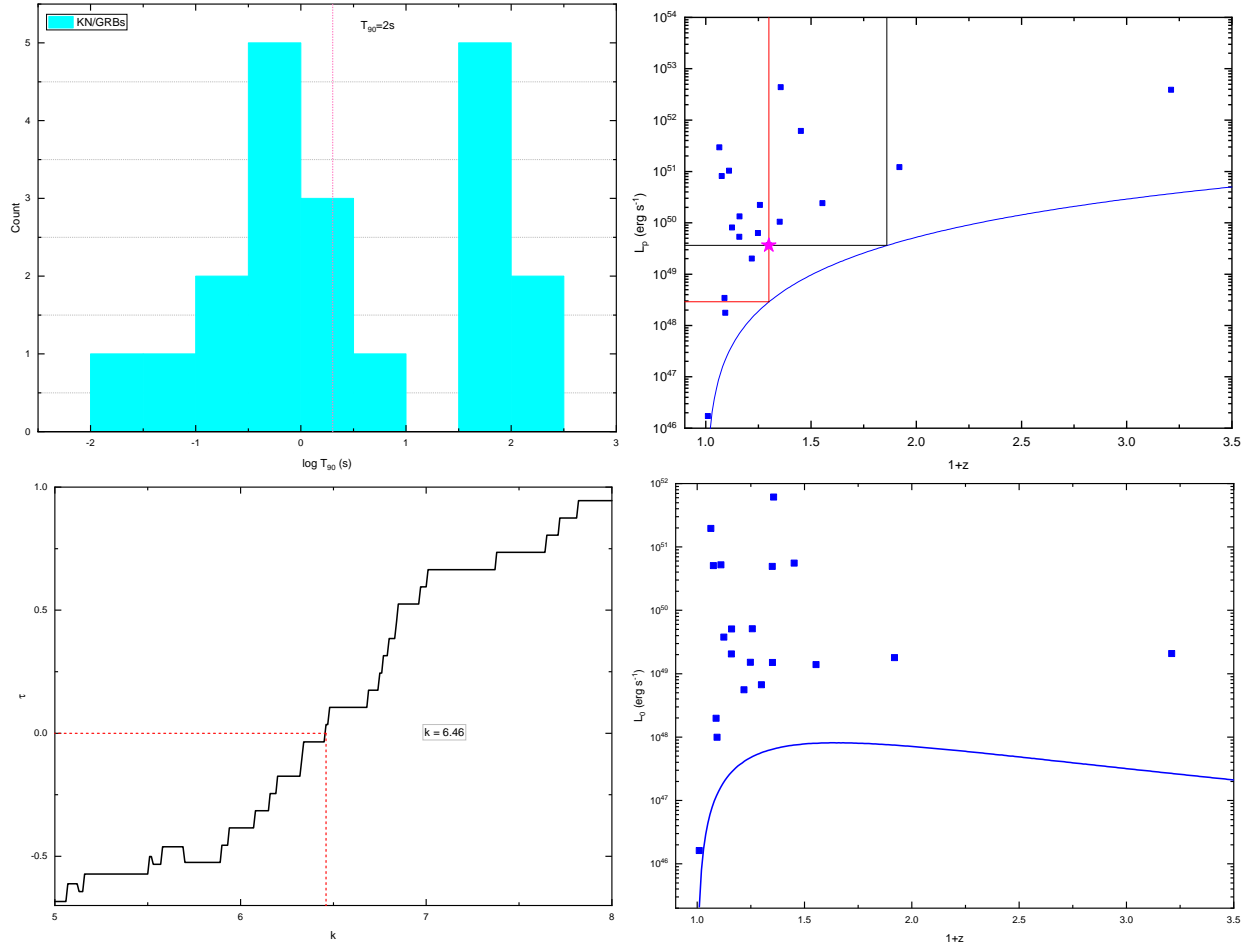


Figure 1. Distributions and correlations for the KN/GRBs sample: Left top: Duration (T_{90}) distribution of KN/GRBs events; Right top: Bolometric luminosity distribution where individual points represent different KN/GRBs, with the line indicating the sensitivity limit of $1.0 \times 10^{-8} \text{ erg cm}^{-2} \text{ s}^{-1}$; Left bottom: In the Kendall τ correlation test, the red dotted line represents the null hypothesis ($\tau = 0$), and the measured correlation strength of $k = 6.46$ suggests that the evolutionary dependence between luminosity and redshift has been effectively removed; Right bottom: De-evolved luminosity function following $L = L_0(1+z)^{6.46}$ for our sample of 20 KN/GRBs, removing the redshift evolution component.

4. DISCUSSIONS AND CONCLUSIONS

In this work, we compile a sample of 20 GRBs that have been securely associated with KN from the literature. one would expect KN/GRBs — being directly connected to the binary compact object merger — to follow the delay SFR more closely than the general sGRB population. Utilizing Lynden-Bell’s C^- method to eliminate the redshift-luminosity correlation, we derive the intrinsic LF and FR of 20 KN/GRBs. This enables us to perform a robust comparison between the KN/GRBs event rate and the delay SFR. Our key findings are as follows: (1) A Kendall τ test yields a statistically significant correlation with a k -value of 6.46 for the 20 KN/GRBs in our sample; (2) The luminosity function distributions of KN/GRBs can be fitted by a smoothly broken power-law (BPL) function. The broken luminosities are around $1.15 \times 10^{49} \text{ erg s}^{-1}$. (3) We observe a decrease trend in the KN/GRBs event rate at low redshifts ($z < 1$). These results suggest that the observed KN/GRBs event rate can’t trace SFR and delay SFR. and may instead point to intrinsic differences in the GRB progenitor population or its dependence on environmental factors.

It is well established that GRBs originate from two primary channels: the mergers of compact binaries (Paczynski 1986) or the core collapse of massive stars (Woosley 1993). The conventional paradigm holds that a subset of IGRBs arises from core-collapse events, often accompanied by supernova-like emission signatures (Galama et al. 1998; Hjorth et al. 2003). Due to their association with massive star formation, IGRBs are widely regarded as powerful probes of

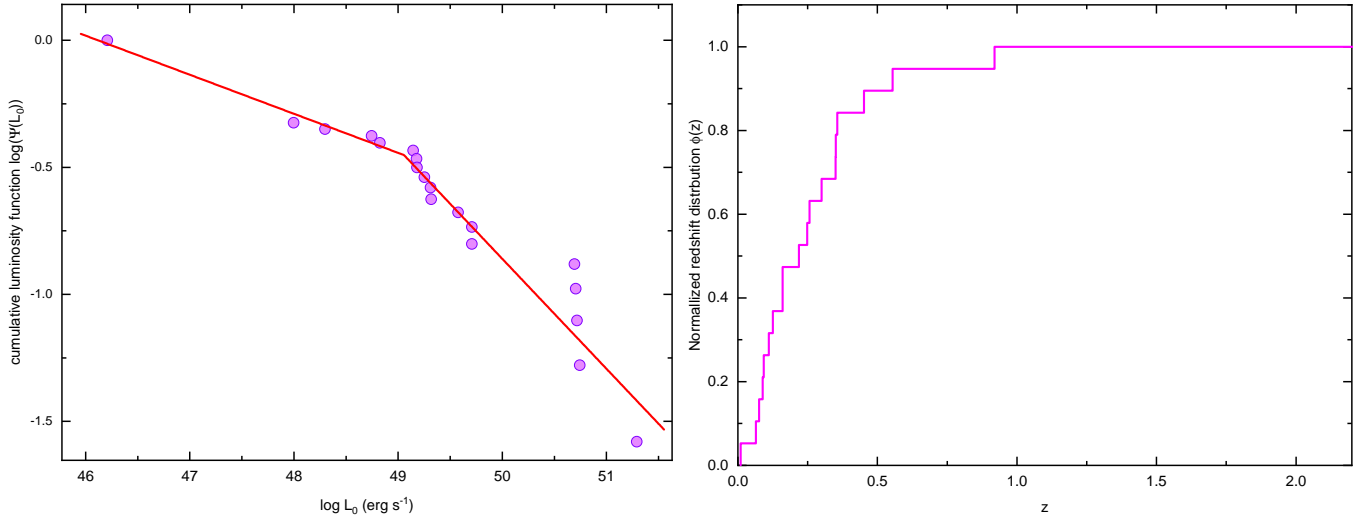


Figure 2. Left: The distribution of cumulative luminosity function $\psi(L_0)$, which is normalized to unity at the lowest luminosity. The function is fitted by red solid line with broken power law. The luminosity function can be expressed as $\psi(L_0) = L_0^{-0.15 \pm 0.04}, L_0 < L_0^b$ and $\psi(L_0) = L_0^{-0.43 \pm 0.03}, L_0 > L_0^b$; Right: Normalized cumulative redshift distribution.

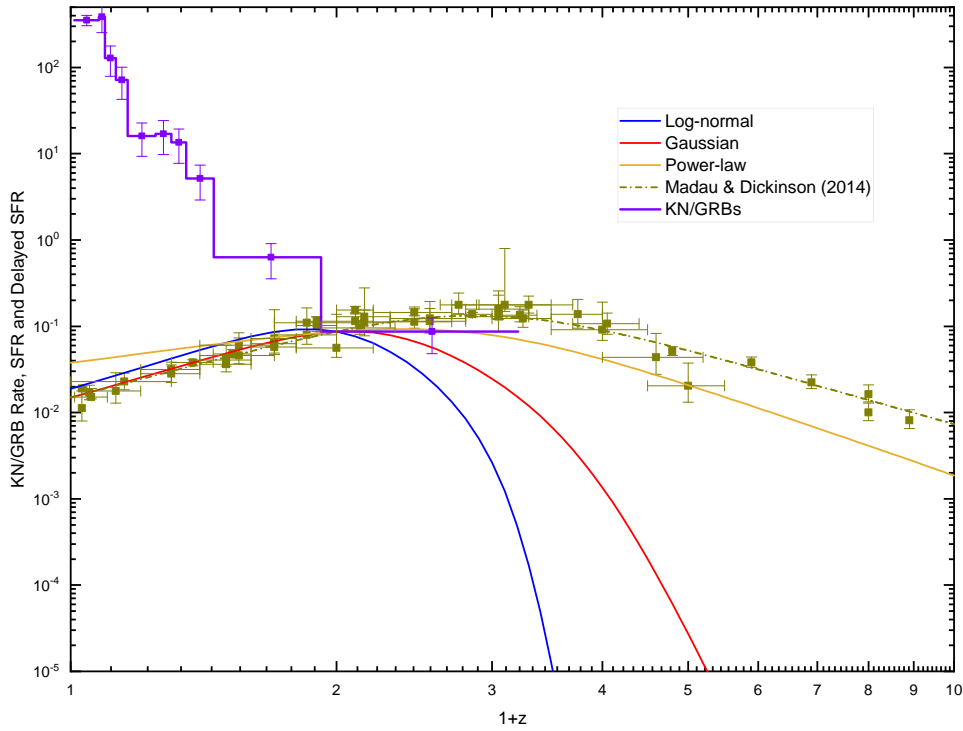


Figure 3. Comparison KN/GRBs rate and SFR. The thick colored curves display the best fits achieved by applying merged delay models to each distribution. The SFR data and fit line were collected from [Madau & Dickinson \(2014\)](#) (Brown dots). The blue line are the formation rate of fitting 20 KN/GRBs sources. The error bar gives a 1σ poisson error ([Gehrels 1986](#)). These fitting lines are normalized at $z=1$.

the cosmic SFR at high redshifts. However, previous studies have revealed a discrepancy between the observed lGRB FR and the SFR, with some suggesting contamination from compact binary merger events ([Yu et al. 2015](#); [Petrosian et al. 2015](#); [Petrosian & Dainotti 2024](#)). Intriguingly, [Li et al. \(2025\)](#) calculated the event rate of GRBs associated with supernovae and still found a significant excess at low redshifts. This suggests that the low-redshift excess cannot be fully explained by progenitor channel mixing alone. Our findings also offer additional support for this viewpoint.

Further evidence for complexity in the GRB population comes from luminosity-dependent studies. Dong et al. (2023) found that the event rates of low-luminosity lGRBs exceed the SFR, whereas high-luminosity lGRBs are in excellent agreement with the cosmic star formation history. Similarly, Liu et al. (2025) noted that the rates of medium and faint GRBs exceed the SFR at low redshifts, while the rate of bright GRBs closely follows the SFR. These findings indicate that the low-redshift excess in the GRB rate is likely driven by luminosity-dependent effects or environmental factors, rather than being solely attributable to the distinction between compact binary mergers and core-collapse supernovae.

Extra explanations for this discrepancy include the small size of the current KN/GRBs sample. The current sample is deficient in high-redshift ($z > 1$) KN/GRBs, with only one detected events in the $z > 2$ range, leading to considerable uncertainty. Future observations will be crucial for exploring the relationship between the KN/GRB FR and the delayed SFR in the high-redshift universe.

ACKNOWLEDGEMENTS

This work was supported by the Postdoctoral Fellowship Program of CPSF under Grant Number GZC20252095, the China Postdoctoral Science Foundation under Grant Number 2025M773194, Caiyun Postdoctoral Program in Yunnan Province of China (grant No. C615300504124), the National Natural Science Foundation of China (grant Nos. 12503040, 11933008 and 12303040), National Key R&D Program of China (grant No. 2022YFE0116800), and Yunnan Fundamental Research Projects (grant NOS. 202501AS070055, 202503AP140013, 202201AT070092 and 202401AT070143).

REFERENCES

Abbott, B. P., Abbott, R., Abbott, T. D., et al. 2017a, ApJL, 848, L13

—. 2017b, ApJL, 848, L12

Ahumada, T., Singer, L. P., Anand, S., et al. 2021, Nature Astronomy, 5, 917

Ando, S. 2004, JCAP, 2004, 007

Arcavi, I., Hosseinzadeh, G., Howell, D. A., et al. 2017, Nature, 551, 64

Band, D., Matteson, J., Ford, L., et al. 1993, ApJ, 413, 281

Blain, A. W., & Natarajan, P. 2000, MNRAS, 312, L35

Bloom, J. S., Frail, D. A., & Sari, R. 2001, AJ, 121, 2879

Bromberg, O., Nakar, E., Piran, T., & Sari, R. 2013, ApJ, 764, 179

Chen, J. H., Jia, X. D., Dong, X. F., & Wang, F. Y. 2024, ApJL, 973, L54

Coward, D. 2007, NewAR, 51, 539

Dalessi, S., Roberts, O. J., Meegan, C., & Fermi GBM Team. 2023, GRB Coordinates Network, 33411, 1

Deng, C.-M., Wei, J.-J., & Wu, X.-F. 2019, Journal of High Energy Astrophysics, 23, 1

Dong, X. F., Zhang, Z. B., Li, Q. M., Huang, Y. F., & Bian, K. 2023, ApJ, 958, 37

Du, X. Y., Zhang, Z. B., Du, W. C., et al. 2025, ApJL, 987, L13

Efron, B., & Petrosian, V. 1992, ApJ, 399, 345

Eichler, D., Livio, M., Piran, T., & Schramm, D. N. 1989, Nature, 340, 126

Elliott, J., Greiner, J., Khochfar, S., et al. 2012, A&A, 539, A113

Fynbo, J. P. U., Watson, D., Thöne, C. C., et al. 2006, Nature, 444, 1047

Galama, T. J., Vreeswijk, P. M., van Paradijs, J., et al. 1998, Nature, 395, 670

Gehrels, N. 1986, ApJ, 303, 336

Gehrels, N., Norris, J. P., Barthelmy, S. D., et al. 2006, Nature, 444, 1044

Golenetskii, S., Aptekar, R., Mazets, E., et al. 2006, GRB Coordinates Network, 5890, 1

—. 2007, GRB Coordinates Network, 6615, 1

Golenetskii, S., Aptekar, R., Frederiks, D., et al. 2010, GRB Coordinates Network, 10890, 1

—. 2013, GRB Coordinates Network, 14771, 1

Greiner, J., Krühler, T., Fynbo, J. P. U., et al. 2009, ApJ, 693, 1610

Hjorth, J., Sollerman, J., Møller, P., et al. 2003, Nature, 423, 847

Jin, Z.-P., Zhou, H., Covino, S., et al. 2021, arXiv e-prints, arXiv:2109.07694

Kann, D. A., Rossi, A., Oates, S. R., et al. 2024, A&A, 684, A164

Kasen, D., Metzger, B., Barnes, J., Quataert, E., & Ramirez-Ruiz, E. 2017, Nature, 551, 80

Kouveliotou, C., Meegan, C. A., Fishman, G. J., et al. 1993, ApJL, 413, L101

Li, L.-X., & Paczyński, B. 1998, ApJL, 507, L59

Li, Q.-M., & Sun, Q.-B. 2025, ApJ, 978, 160

Li, Q.-M., Sun, Q.-B., Qian, S.-B., & Li, F.-X. 2025, ApJL, 990, L54

Li, Q. M., Zhang, Z. B., Han, X. L., et al. 2023, MNRAS, 524, 1096

Lin, H.-N., Li, X.-Y., & Zou, R. 2024, ApJ, 969, 123

Liu, Y., Zhang, Z. B., Dong, X. F., Li, L. B., & Du, X. Y. 2025, MNRAS, 542, 215

Lynden-Bell, D. 1971, MNRAS, 155, 95

MacFadyen, A. I., & Woosley, S. E. 1999, ApJ, 524, 262

Madau, P., & Dickinson, M. 2014, ARA&A, 52, 415

Maloney, A., & Petrosian, V. 1999, ApJ, 518, 32

Mangan, J., Dunwoody, R., Meegan, C., & Fermi GBM Team. 2021, GRB Coordinates Network, 31210, 1

McGlynn, S., Foley, S., McBreen, S., et al. 2008, A&A, 486, 405

Metzger, B. D. 2017, Living Reviews in Relativity, 20, 3

Narayan, R., Paczynski, B., & Piran, T. 1992, ApJL, 395, L83

Paczynski, B. 1986, ApJL, 308, L43

Paczyński, B. 1998, ApJL, 494, L45

Paul, D. 2018, MNRAS, 477, 4275

Petrosian, V. 1992, in Statistical Challenges in Modern Astronomy, 173–200

Petrosian, V., & Dainotti, M. G. 2024, ApJL, 963, L12

Petrosian, V., Kitanidis, E., & Kocevski, D. 2015, ApJ, 806, 44

Piran, T., & Guetta, D. 2006, in American Institute of Physics Conference Series, Vol. 836, Gamma-Ray Bursts in the Swift Era, ed. S. S. Holt, N. Gehrels, & J. A. Nousek (AIP), 58–63

Rastinejad, J., Fong, W.-f., Gompertz, B. P., et al. 2022, Solidifying the Origin of a Possible Kilonova at 350 Mpc, HST Proposal. Cycle 29, ID. #16923

Rosswog, S. 2005, ApJ, 634, 1202

Sakamoto, T., Barthelmy, S. D., Barbier, L., et al. 2008, ApJS, 175, 179

Salvaterra, R., Della Valle, M., Campana, S., et al. 2009, Nature, 461, 1258

Singal, J., Ko, A., & Petrosian, V. 2014, ApJ, 786, 109

Stanbro, M., & Meegan, C. 2016, GRB Coordinates Network, 19843, 1

Stanek, K. Z., Matheson, T., Garnavich, P. M., et al. 2003, ApJL, 591, L17

Stratta, G., Nicuesa Guelbenzu, A. M., Klose, S., et al. 2025, ApJ, 979, 159

Sun, H., Zhang, B., & Li, Z. 2015, ApJ, 812, 33

Tanvir, N. R., Fox, D. B., Levan, A. J., et al. 2009, Nature, 461, 1254

Totani, T. 1997, ApJL, 486, L71

—. 1999, ApJ, 511, 41

Wanderman, D., & Piran, T. 2015, MNRAS, 448, 3026

Wang, Y., Xia, Z.-Q., Zheng, T.-C., Ren, J., & Fan, Y.-Z. 2023, ApJL, 953, L8

Wijers, R. A. M. J., Bloom, J. S., Bagla, J. S., & Natarajan, P. 1998, MNRAS, 294, L13

Woosley, S. E. 1993, ApJ, 405, 273

Wu, S.-W., Xu, D., Zhang, F.-W., & Wei, D.-M. 2012, MNRAS, 423, 2627

Yang, J., Ai, S., Zhang, B.-B., et al. 2022, Nature, 612, 232

Yang, Y.-H., Troja, E., O'Connor, B., et al. 2024, Nature, 626, 742

Yu, H., Wang, F. Y., Dai, Z. G., & Cheng, K. S. 2015, ApJS, 218, 13

Zeh, A., Klose, S., & Hartmann, D. H. 2004, ApJ, 609, 952

Zeng, H., Petrosian, V., & Yi, T. 2021, ApJ, 913, 120

Zhang, B., Zhang, B.-B., Virgili, F. J., et al. 2009, ApJ, 703, 1696

Zhang, B. B., Liu, Z. K., Peng, Z. K., et al. 2021, Nature Astronomy, 5, 911

Zhang, Z. B., Zhang, C. T., Zhao, Y. X., et al. 2018, PASP, 130, 054202

Zhou, H., Jin, Z.-P., Covino, S., et al. 2023, ApJ, 943, 104

Zhu, Y.-M., Zhou, H., Wang, Y., et al. 2023, MNRAS, 521, 269

Table 1. 20 KN/GRBs Included in Our analysis

GRB	T_{90} (s)	z	α	β	E_p (keV)	$E_{\min}-E_{\max}$ (keV)	F (ph/cm ² /s)	L_p $erg\ s^{-1}$	ref
(1)	(2)	(3)	(4)	(5)	(6)	(7)	(8)	(9)	(10)
050709	0.07	0.1606	-0.7	-	83^{+18}_{-18}	30-400	$12.1^{+0.4}_{-0.4}$	$1.33^{+0.04}_{-0.04} \times 10^{50}$	Zhang et al. (2018)
050724	96	0.257	-2.02	-	78.91^{+8}_{-8}	15-150	$3.35^{+0.31}_{-0.31}$	$2.23^{+0.21}_{-0.21} \times 10^{50}$	Zhang et al. (2018)
060505	4	0.089	-0.627	-	124.925	15-150	$1.29^{+0.2}_{-0.24}$	$3.43^{+0.53}_{-0.64} \times 10^{48}$	swift website
060614A	108	0.125	-1.82	-	$134.1^{+24.2}_{-24.2}$	15-150	$11.4^{+0.7}_{-0.7}$	$8.05^{+0.49}_{-0.49} \times 10^{49}$	Zhang et al. (2018)
061201	0.76	0.111	-0.3	-	873^{+458}_{-284}	20-3000	$3.19^{+0.72}_{-2.72} \times 10^{-5a}$	$1.03^{+0.23}_{-0.88} \times 10^{51}$	Golenetskii et al. (2006)
070707	1	0.35	-0.57	-	427^{+374}_{-144}	20-2000	$8.1^{+2.9}_{-6.7} \times 10^{-6a}$	$3.41^{+1.22}_{-2.82} \times 10^{51}$	Golenetskii et al. (2007)
070714B	64	0.92	-0.88	-	$81.62^{+36.76}_{-36.76}$	15-150	$2.75^{+0.16}_{-0.16}$	$1.21^{+0.07}_{-0.07} \times 10^{51}$	Du et al. (2025)
070809	1.39	0.2187	-1.33	-	145.5^{+70}_{-70}	15-150	$0.97^{+0.12}_{-0.12}$	$2.00^{+0.25}_{-0.25} \times 10^{49}$	Zhang et al. (2018)
080503	170	0.3	-1.23	-	226.61	15-150	$0.67^{+0.13}_{-0.13}$	$3.63^{+0.71}_{-0.71} \times 10^{49}$	Du et al. (2025)
100625A	0.33	0.452	-0.1	-	414^{+128}_{-78}	20-2000	$8.1^{+1.5}_{-1.5} \times 10^{-6a}$	$6.16^{+1.14}_{-1.14} \times 10^{51}$	Golenetskii et al. (2010)
111117A	0.47	2.211	-0.69	-	370^{+37}_{-37}	15-150	$2.8^{+0.2}_{-0.2}$	$3.89^{+0.28}_{-0.28} \times 10^{52}$	Zhang et al. (2018)
130603B	0.18	0.3564	-0.73	-	660^{+100}_{-100}	20-10000	$1^{+0.2}_{-0.2} \times 10^{-4a}$	$4.37^{+0.87}_{-0.87} \times 10^{52}$	Golenetskii et al. (2013)
140903A	0.3	0.351	-1.36	-	$44.17^{+16.2}_{-16.2}$	15-150	$2.5^{+0.2}_{-0.2}$	$1.05^{+0.08}_{-0.08} \times 10^{50}$	Zhang et al. (2018)
150101B	0.018	0.093	-0.58	-	96.55	15-150	$0.73^{+0.3}_{-0.3}$	$1.76^{+0.72}_{-0.72} \times 10^{48}$	Du et al. (2025)
160821B	0.48	0.16	-1.37	-	84^{+19}_{-19}	10-1000	$9.16^{+1.19}_{-1.19}$	$5.32^{+0.69}_{-0.69} \times 10^{49}$	Stanbro & Meegan (2016)
170817A	2	0.009783	-0.89	-	82^{+21}_{-21}	8-1000	$1.9^{+0.2}_{-0.2}$	$1.72^{+0.18}_{-0.18} \times 10^{46}$	GCN Circular 21520
191019A	64.35	0.248	-1.99	-	$1.19^{+0.2}_{-0.2}$	15-150	$2.15^{+0.06}_{-0.06}$	$6.33^{+0.18}_{-0.18} \times 10^{49}$	swift website
200522A	0.62	0.554	-0.53	-	77.76	15-150	2.02	2.40×10^{50}	swift website
211211A	34.3	0.076	-1.3	-2.4	$646.8^{+7.8}_{-7.8}$	10-1000	$324.9^{+1.5}_{-1.5}$	$8.12^{+0.04}_{-0.04} \times 10^{50}$	Mangan et al. (2021)
230307A	35	0.0646	-1.07	-	936^{+3}_{-3}	10-1000	791^{+4}_{-4}	$2.93^{+0.01}_{-0.01} \times 10^{51}$	Dalessi et al. (2023)

Note: References for the spectral parameters (E_p , α , β , peak flux , E_{\max} , and redshift of GRB 080503, GRB 070707: <https://www.mpe.mpg.de/~jcg/grbgen.html> ; a: These peak fluxes are in units of $erg\ cm^{-2}\ s^{-1}$. b: The redshift of GRB 070707 and GRB 080503 were assumed as 0.35 and 0.3 (McGlynn et al. 2008; Zhou et al. 2023). The data of GRB 060505, 191019A and GRB 200522A were acquired from The Swift/BAT Gamma-Ray Burst website: <https://swift.gsfc.nasa.gov/results/batgrbcat/>.